J|A|C|S
ARTICLES
Published on Web 04/25/2002

Measurements of the Photodissociation Quantum Yields of MbNO and MbO_2 and the Vibrational Relaxation of the Six-Coordinate Heme Species

Xiong Ye, Andrey Demidov, and Paul M. Champion*

Contribution from the Physics Department and Center for Interdisciplinary Research on Complex Systems, Northeastern University, Boston, Massachusetts 02115

Received October 23, 2001

Abstract: The ($t \sim 0$) photodissociation quantum yields (Y_0) of MbNO and MbO_2 are measured to be 50 $\pm$ 5 and 28 $\pm$ 6%, respectively, using MbCO ($Y_0 = 100\%$) as a reference. When photolysis does not take place, we find that a significant portion of the photon energy contributes to heating of the residual six-coordinate heme (MbNO* and MbO_2*). The time constant for vibrational relaxation of the six-coordinate ligand-bound heme is found to be close to 1 ps for both samples. The MbO_2 sample also shows a ~4-ps optical response that is assigned to a rapid phase (25−30% amplitude) of O_2 geminate rebinding. We observe no additional geminate recombination in the MbO_2 sample out to 120 ps. In contrast, the MbNO sample displays significant geminate recombination over the first 120 ps, which can be adequately fit with two exponentials whose amplitudes and time constants appear to depend weakly on the pump wavelength. This more complex kinetic behavior conceivably arises due to heating of the photodissociated heme and its effect on the geminate recombination as the system cools. Overall, the data are consistent with a hypothesis that distortions along the iron−ligand bending coordinate play a key role in the photodissociation process. The transient formation of an unphotolyzable FeO_2 side-on binding geometry is suggested to be responsible for the lowered quantum yield of MbO_2 relative to MbNO.

Introduction

Myoglobin (Mb) is the oxygen storage protein in mammalian muscle tissues. Its functionality for binding diatomic ligands is carried out by the heme prosthetic group. The iron atom at the center of the heme is covalently bound to the "proximal" histidine residue of the protein backbone. The protein provides a hydrophobic pocket around the heme, so that the iron can reversibly bind small ligands such as O_2, CO, and NO to its "distal" side.

Each of the above diatomic ligands has been found to be photodissociable.[1] This makes it possible to study ligand binding kinetics with flash photolysis. Early studies observed a significant difference in photolysis efficiency (or "quantum yield") among the ligands.[1,2] At this point, we note that the term "quantum yield" can be used in different contexts. In this paper, we refer to the most fundamental definition. That is, the probability (Y_0) of ligand dissociation (at $t = 0$) following the absorption of a *single* photon. In some studies, the term has been used under conditions of multiple photon excitation or at longer time scales where partial (or complete) geminate recombination has taken place and the term "bimolecular dissociation yield" may be more appropriate. The three standard methods used for the measurement[3] of ligand photolysis are (i) the kinetic method, (ii) the steady-state method, and (iii) the pulse photolysis method. The first two methods are focused on bimolecular rebinding and use constant illumination, so that either the rates of transition between the photostationary states or the equilibrium ligand binding curves are measured. The measured rate is the sum of the association and dissociation rates, and the yield is the overall "bimolecular dissociation yield". The pulse photolysis method utilizes a pulse that is short compared to the ligand recombination time. Early work utilized pulse widths in the millisecond to microsecond range, which was sufficient to measure bimolecular dissociation yields. Further studies with nanosecond or faster time resolution found that a photodissociated ligand can remain in the heme pocket and geminately recombine.[4−7] The bimolecular dissociation yield is then expressed as $Y_b = \eta Y_0$, where Y_0 is the ($t \sim 0$) photodissociation yield (sometimes referred to as the intrinsic quantum yield) and η is the fraction of ligands that escape to solvent and do not undergo geminate rebinding. The variations in the

* Author to whom correspondence should be addressed. E-mail: champ@neu.edu.

(1) Gibson, Q. H.; Ainsworth, S. *Nature* **1957**, *180*, 1416.
(2) Antonini, E.; Brunori, M. *Hemoglobin and myoglobin in their reactions with ligands*; North-Holland Publishing Co.: Amsterdam, 1971; Vol. 21.
(3) Brunori, M.; Giacometti, G. M. *Methods Enzymol.* **1981**, *76*, 582−595.
(4) Ansari, A.; DiIorio, E. E.; Dlott, D. D.; Frauenfelder, H.; Iben, I. E. T.; Langer, P.; Roder, H.; Sauke, T. B.; Shyamsunder, E. *Biochemistry* **1986**, *25*, 3139−3146.
(5) Gibson, Q. H.; Olson, J. S.; Mckinnie, R. E.; Rohlfs, R. J. *J. Biol. Chem.* **1986**, *261*, 228−239.
(6) Henry, E. R.; Sommer, J. H.; Hofrichter, J.; Eaton, W. A. *J. Mol. Biol.* **1983**, *166*, 443−451.
(7) Jongeward, K. A.; Magde, D.; Taube, D. J.; Marsters, J. C.; Traylor, T. G.; Sharma, V. S. *J. Am. Chem. Soc.* **1988**, *110*, 380−387.

10.1021/ja017359n CCC: $22.00

bimolecular dissociation yields observed for NO ($Y_b < 10^{-3}$),[1] CO ($Y_b = 0.95$),[6] and O_2 ($Y_b = 0.057$ or 0.13)[5,8] are ascribed to η (and differences in the geminate recombination rates), while it is often assumed that the ($t \sim 0$) quantum yield is unity for all three ligands.[8,9]

However, it has been noted that, when the bimolecular and geminate phase of O_2 rebinding is analyzed up to the nanosecond and picosecond regime, there is still about 60−70% of the "photolyzed" amplitude that is not accounted for.[8] Independent picosecond experiments have also found the "effective" picosecond quantum yield in MbNO and MbO_2 to be much lower than unity.[10−12] Geminate recombination processes have been proposed to be responsible for the "missing amplitude",[8,9,13] suggesting that an excited intermediate of the five-coordinate heme can rebind NO and O_2 on ultrafast (100 fs to 2 ps) time scales. The ultrafast geminate recombination hypothesis can potentially account for the significant (∼50−80%) reduction in the photodissociation quantum yield measured on longer time scales. However, an alternative explanation is that the intrinsic ($t \sim 0$) quantum yield (Y_0) is ligand dependent and less than unity for MbNO and MbO_2. In the present paper, we demonstrate that for MbNO and MbO_2 there are other channels of direct energy relaxation that compete with the ligand dissociation channel and lead to $Y_0 < 1$ along with heating of the residual six-coordinate heme.

Molecular dynamics simulation studies on myoglobin and cytochrome *c* have shown how photon absorption leads to local heating of the heme followed by cooling. Theoretical time constants range from 1−4 and 20−40 ps for biphasic cooling[14] to 6 ps for monophasic cooling.[15] A model using classical thermal diffusion theory also points to initial heme cooling taking place with a time constant of less than 4 ps.[16] Recent studies on cytochrome *c*[17] have shown that methionine ligand photodissociation followed by ∼6-ps geminate recombination takes place in this system, complicating the ability to extract a pure thermal response. However, time-resolved resonance Raman spectroscopy has been used to monitor the mode-specific cooling of the photoexcited deoxyheme of Mb[18] and the vibrational relaxation time was estimated to be 2−5 ps. Another time-resolved resonance Raman study[19] measured heme cooling upon photodissociation of carbomonoxymyoglobin (which is free from geminate recombination on ps time scales) and found that a vibrational relaxation time constant of 1.9 ps dominated the process of ν_4 band population decay (ν_4 is the heme ring "breathing" mode). A more recent transient absorption study of deoxyMb in the Q-band and band III regions found that the dominating amplitude for vibrational cooling of the hot electronic ground state has a time constant in the range of 1.5−4.5 ps.[20]

We also performed investigations of the transient absorption of the deoxy-Mb and MbCO photoproducts and observed the Soret band line shape evolution of the hot deoxy product state (Mb*). A moment analysis of the spectral evolution shows a ∼0.4-ps fast phase involving line narrowing and a slower phase (∼4 ps) involving a shift of the absorption maximum from red to blue.[21] Experiments on metal porphyrin model compounds also observe a spectrum of the hot porphyrin that is red-shifted.[22]

In the present paper, we emphasize that the electronic ground state of the six-coordinate *ligated* heme can also be vibrationally excited (e.g., in states we denote as MbNO* and MbO_2*) through internal conversion of the photon energy when the ligand does not photodissociate. Our studies have revealed no compelling evidence for the existence of an intermediate electronic excited state[9] that recombines on ultrafast time scales. Moreover, we have shown[21] that the ultrafast optical response within the first few picoseconds can be fully described by the vibrational relaxation and cooling of the heme. The analysis we present for MbNO and MbO_2 is consistent with an intrinsic ($t \sim 0$) photodissociation quantum yield for these two samples that is significantly less than unity.

Materials and Methods

Sample Preparation. Horse heart myoglobin was obtained from Sigma Inc. and a metMb solution was prepared using 100 mM potassium phosphate buffer (pH 7.0) at room temperature. The metMb solution was degassed with argon for 1 h, and an equimolar quantity of 1 M sodium dithionite was added to obtain deoxyMb. MbNO was prepared by further addition of an equimolar quantity of 1 M degassed sodium nitrite solution to the deoxyMb sample in the presence of 1 M sodium dithionite. The CO-bound Mb was prepared by flushing CO gas over the surface of the deoxyMb sample for 1 h. The oxygen-bound Mb was prepared by adding 1 M sodium dithionite to metMb in open air followed by passage through a G25 column to eliminate excess sodium dithionite. In all cases, the sample concentration was adjusted to have a Soret peak absorption of ∼1 OD in a 1-mm path length cell. The absorption spectra were measured before and after each experiment with a spectrophotometer (Hitachi U-3410) to check sample quality and stability. All samples were placed in an anaerobic spinning cell having a 2-in.-diameter and a 1-mm path length. The cell was rotated at ∼7000 rpm using a brushless high-tolerance motor (Maxon Precision Motors, Inc.).

System Setup and Detection Methods. We use an amplified Ti: sapphire laser (REGA 9050, Coherent, Inc.). Details and schematics of this system can be found elsewhere.[17] The amplified laser system generates ∼50-fs laser pulses at ∼800 nm with a repetition rate of 250 kHz and an average power of ∼1 W. These fundamental pulses are used to pump an optical parametric amplifier (OPA) as well as to generate the second harmonic (400 nm) and the white light continuum. The white light continuum is generated in a spinning fused-silica disk with the 800 nm pump pulse and its spectrum covers the range from 390 nm to over 800 nm. The OPA pulses are ∼50 fs with the 250-kHz repetition rate and can be tuned from about 520 to 650 nm. Both the 400-nm second harmonic and the OPA outputs are used as pump pulses. Their timing with respect to the probe pulses (white light continuum) is controlled using a motorized translation stage (Melles Griot, Inc.).

(8) Walda, K. N.; Liu, X. Y.; Sharma, V. S.; Magde, D. *Biochemistry* **1994**, *33*, 2198−2209.
(9) Petrich, J. W.; Poyart, C.; Martin, J. L. *Biochemistry* **1988**, *27*, 4049−4060.
(10) Reynolds, A. H.; Rand, S. D.; Rentzepis, P. M. *Proc. Natl. Acad. Sci. U.S.A.* **1981**, *78*, 2292−2296.
(11) Carver, T. E.; Rohlfs, R. J.; Olson, J. S.; Gibson, Q. H.; Blackmore, R. S.; Springer, B. A.; Sligar, S. G. *J. Biol. Chem.* **1990**, *265*, 20007−20020.
(12) Dzhagarov, B. M.; Kruk, N. N.; Tikhomirov, S. A.; Galievsky, V. A. In *Ultrafast Processes in Spectroscopy*; Svelto, O., De Silvestri, S., Denardo, G., Eds.; Plenum Press: New York, 1996; 497−502.
(13) Olson, J. S.; Phillips, G. N., Jr. *J. Biol. Chem.* **1996**, *271*, 17593−17596.
(14) Henry, E. R.; Eaton, W. A.; Hochstrasser, R. M. *Proc. Natl. Acad. Sci. U.S.A.* **1986**, *83*, 8982−8986.
(15) Sagnella, D. E.; Straub, J. E. *J. Phys. Chem. B* **2001**, *105*, 7057−7063.
(16) Li, P.; Champion, P. M. *Biophys. J.* **1994**, *66*, 430−436.
(17) Wang, W.; Ye, X.; Demidov, A. A.; Rosca, F.; Sjodin, T.; Cao, W.; Sheeran, M.; Champion, P. M. *J. Phys. Chem. B* **2000**, *104*, 10789−10801.
(18) Lingle, R.; Xu, X. B.; Zhu, H. P.; Yu, S. C.; Hopkins, J. B. *J. Phys. Chem.* **1991**, *95*, 9320−9331. Li, P.; Sage, J. T.; Champion, P. M. *J. Chem. Phys.* **1992**, *97*, 3214−3227.
(19) Mizutani, Y.; Kitagawa, T. *Science* **1997**, *278*, 443−446.
(20) Kholodenko, Y.; Volk, M.; Gooding, E.; Hochstrasser, R. A. *Chem. Phys.* **2000**, *259*, 71−87.
(21) Ye, X.; Demidov, A. A.; Champion, P. M. In preparation.
(22) Rodriguez, J.; Holten, D. *J. Chem. Phys.* **1989**, *91*, 3525−3531.

The pump and probe beams are focused into the spinning sample cell using an achromatic lens. Care is taken to make the pump beam completely overlap the probe beam at the sample. The beam focal diameters (86.5%) of the pump and probe are 90 and 30 μm, respectively (BeamProfiler, Photon, Inc.). At the sample, the average powers are ~5 mW for the 400-nm pump beam, ~10 mW for the OPA pump beam, and ~10 μW for the white light continuum probe beam (integrated over the bandwidth 400−500 nm). The pump and probe cross-correlation is ~200 fs and is measured using the sample cell filled with buffer solution. Such a measurement is also used to find the zero time delay between the pump and probe pulses as a function of wavelength, so that chirp in the continuum spectrum can be removed.

We used two different detection techniques to measure transient spectra. The first technique uses a diode array (TBY1024 Princeton Instruments, Inc.) as the detector. It is coupled to the axial output port of the monochromator and connected with an optical multichannel analyzer (OMA) controller (Princeton Instruments, Inc.). The spectral window is ~130 nm with a 600 groove/mm grating. A shutter (Uniblitz, Inc.) is used to sequentially block and unblock the pump beam for an equal amount of time (~0.5 s). During the open and closed cycles, the spectra of the probe light (continuum) are collected and averaged, and the net spectrum with the pump on is divided by the net spectrum with the pump blocked. The logarithm of the ratio yields the absolute magnitude of the pump-induced transient absorption difference spectrum.

The second technique is based on the well-known lock-in amplifier method.[23] The pump beam is modulated by a mechanical chopper (3 kHz). A photomultiplier tube (PMT) is attached to the lateral output port of the monochromator and used to detect the signal as the wavelength is scanned by the monochromator. The signal is proportional to both the pump-induced absorption change and the probe light intensity. We use a light stabilizer (Cambridge Research & Instrumentation) that adjusts the probe light power to keep a constant average photocurrent as the detection wavelength is scanned. This works by using the dc part of the PMT output as the feedback control to the light stabilizer.

Chirp Compensation. The effect of differential time delay of the wavelengths in an ultrashort laser pulse is a well-known phenomenon, and there are a number of techniques developed for chirp compensation.[24] We use a set of two prisms and a reflecting mirror that utilize the double-pass principle. This method can be used for chirp compensation in both the pump and probe beams. Unfortunately, this technique is not applicable in the case of white light continuum pulses because of the significantly broader spectral range (~100−150 nm) compared with the spectral bandwidth of a transform-limited femtosecond pulse (~4−10 nm) in the UV−visible region. The main problem arises from the nonlinear dependence of the refractive index of the prism. One way to resolve this problem is to measure the chirp profile as well as a series of sequential spectra with different time delays relative to the pump pulse and then process the data following the chirp profile to determine the time shift of the data points measured at different wavelengths.[17,23] This technique is used in the OMA measurements.

In the case of lock-in detection, we explored another approach that proved to be very successful. We developed software that is able to control simultaneously both the time delay and the monochromator grating and move them along the measured chirp profile. We assume that the "time zero" chirp profile is described by the function $t_0(\lambda)$ and that this function can be well approximated by an n-order polynomial, i.e., $t_0(\lambda) \approx \sum_{i=0}^{n} a_i \lambda^i$. The coefficients α_i are found by measuring the coherence coupling response as a function of wavelength from pure water placed in the sample cell. The coordinates $[\lambda, t_0]$ of the maximums of the water coherence coupling peak are fit by the polynomial to obtain the coefficients α_i. Alternatively, one can use hexane or CS_2 as suggested elsewhere.[25] In the absence of chirp, the transient spectrum ($\Delta A(\lambda,t)$) for a given time delay t would be measured with the translation stage locked at a fixed delay t and only the monocromator gratings would need to be moved. In the presence of the chirp, the transient spectrum ($\Delta A(\lambda, t + t_0(\lambda))$ must be measured differently; i.e., both the grating and the time delay must move simultaneously. In our system, the computer moves the grating to a particular position (λ) and then the computer calculates the corresponding time position for the translation stage, $t + t_0(\lambda)$ and moves it to the correct position for the selected wavelength (λ) and delay time (t).

Determination of Quantum Yield. In the present paper, "quantum yield" is defined as the branching ratio for ligand dissociation following single-photon excitation, prior to any geminate recombination. We use the MbCO sample as a reference for the quantum yield measurements because it has been shown to have a quantum yield of unity.[26,27] The dissociation ratios for NO and O_2 relative to CO are measured between 10 and 25 ps, and the initial ($t = 0$) quantum yields are derived by making extrapolations to $t = 0$, using high-resolution geminate rebinding kinetics measured between 200 fs and 200 ps. (The data are typically fit starting between 200 and 400 fs to avoid complications that can arise from nonlinear coherent coupling signals). The dissociation ratios are derived after straightforward corrections for small differences in pump beam absorption and the relative concentration of the samples. Assuming linear absorption of pump and probe light, the induced absorption change (over the beam path length) is

$$\Delta A(\lambda) = \Delta\epsilon(\lambda) Y_0 J^{\mathrm{abs}}_{\mathrm{pump}} \qquad (1)$$

where $\Delta\epsilon(\lambda)$ is the difference of the extinction coefficients of the product and reactant and $J^{\mathrm{abs}}_{\mathrm{pump}} = J^{0}_{\mathrm{pump}}(1 - 10^{-A_{\mathrm{pump}}})$ is the number of absorbed pump photons per unit area. Here J^{0}_{pump} (in photons/cm^2) is the incident flux integrated over the laser pulse duration and is effectively found by measurement of the absorption change in MbCO (since $Y_0 = 1$). The quantity A_{pump} is the sample absorbance at the pump wavelength. Measurements on MbNO (or MbO_2) and MbCO are performed consecutively to ensure a minimum change in experimental conditions. Experimental probe delays between 10 and 25 ps are utilized to minimize transient heating effects so that $\Delta\epsilon(\lambda)$ can be obtained from the known equilibrium difference spectrum.

Results

Continuum Measurements. In Figure 1 we present the time evolution of the differential absorbance in the Soret band region following photoexcitation at 580 nm. Experiments on samples of deoxyMb and its complex with CO, O_2, and NO are presented. The signals in deoxyMb (Figure 1A) are short-lived and are attributed[21] to vibrational cooling of the hot heme group in Mb*. For MbCO (Figure 1B), the signals are dominated by the Mb − MbCO difference signal and the signal associated with the cooling of deoxyMb* is small in comparison. However, the spectral cooling dynamics of Mb* are superimposed on the Mb − MbCO difference spectrum and account for the small (~300−400 fs) rise in ΔA near 434 nm, as the heme in Mb* undergoes intramolecular vibrational redistribution and the Soret band narrows and intensifies in this region. The rapid (~100 fs) decrease of the antibleach near 420 nm is primarily due to the coherence-coupling signal. There is no evidence of any geminate recombination on short time scales in the MbCO sample (note constant ΔA at 435 nm), supporting the assignment

(23) Rosca, F.; Kumar, A. T. N.; Ye, X.; Sjodin, T.; Demidov, A. A.; Champion, P. M. *J. Phys. Chem.* **2000**, *104*, 4280−4290.
(24) *Femtosecond Laser Pulses. Principles and Experiments*; Rullière, C., Ed.; Springer: Berlin, 1998; pp 1−309.
(25) Yamaguchi, S.; Hamaguchi, H.-O. *Appl. Spectrosc.* **2000**, *49*, 1513−1515.
(26) Bucher, T.; Kaspers, J. *Biochim. Biophys. Acta* **1947**, *1*, 21−34.
(27) Schuresko, D. D.; Webb, W. W. *Biophys. J.* **1978**, *24*, 382−383.

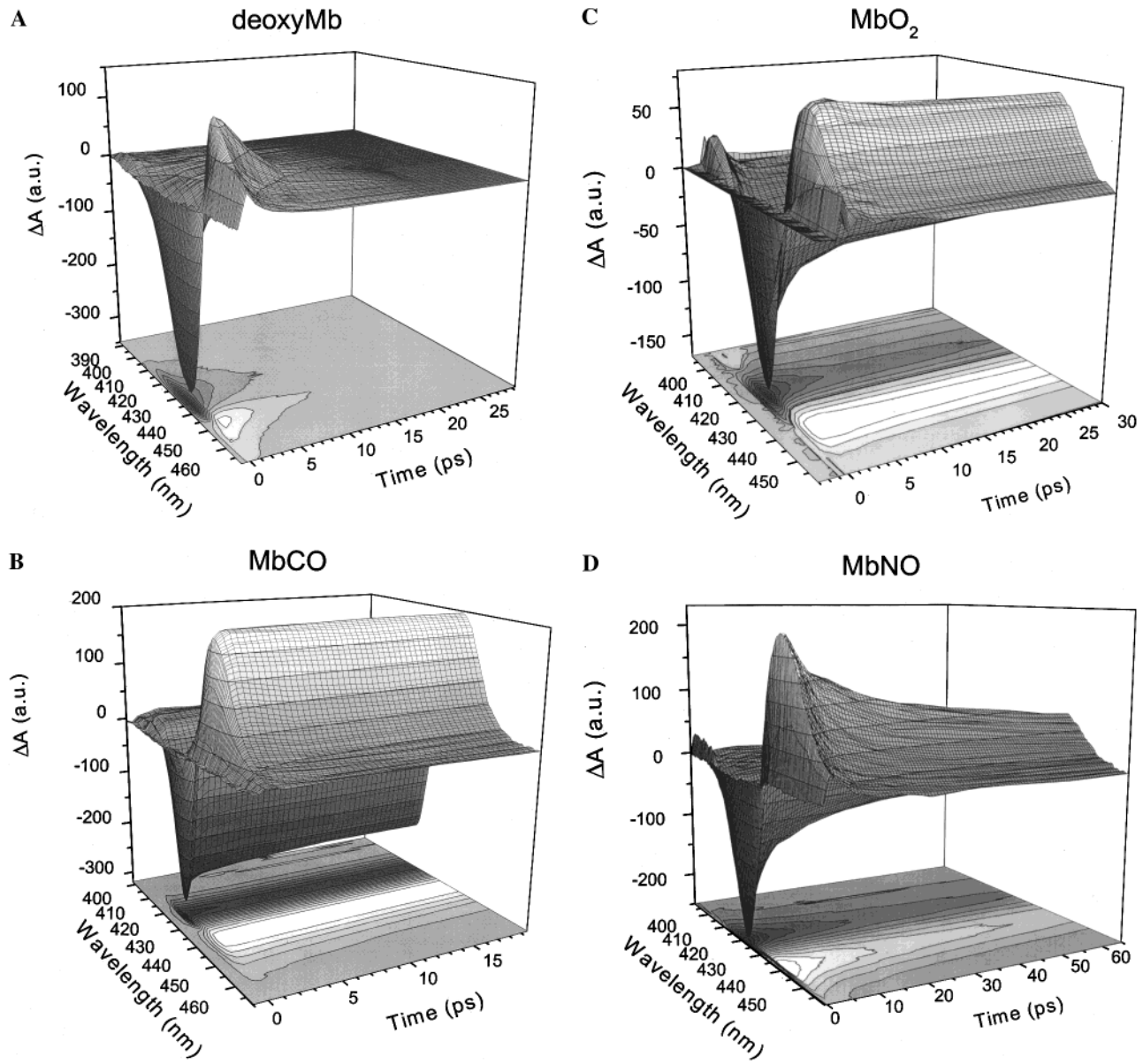

Figure 1. (A−D) Transient spectra of various myoglobin samples pumped at 580 nm. In this and the following figures, au stands for arbitrary units. In this figure, the ordinate values are proportional to the lock-in amplifier read-out in microvolts, while in the following figures, the ordinate has been renormalized to accommodate the fitting procedure.

of unity quantum yield out to the nanosecond time regime where a small geminate rebinding phase can be observed.[6,28]

In Figure 1C and D, we display the spectral dynamics for samples of MbO_2 and MbNO, respectively In these samples, there are several processes that take place simultaneously: (i) there are the initial bleaching ($\Delta A < 0$) and antibleaching ($\Delta A > 0$) signals that arise from ligand photolysis; (ii) there is a signal due to geminate ligand recombination that is characterized by the *simultaneous* change in ΔA at the peaks of the bleach and antibleach (this signal is particularly evident for MbNO); and (iii) there are spectral cooling signals that arise from Mb* *and* from the residual six-coordinate heme material that has absorbed a photon but *not* dissociated ligand. This latter signal is particularly evident for MbO_2 near 420 nm because there is only a relatively small amount of O_2 geminate recombination competing with the cooling signal from the MbO_2* Soret band. The distinct decrease in the bleaching signal near 420 nm in Figure 1C (without a concomitant change in the antibleach at 434 nm) is a characteristic of the hot (and broadened) six-coordinate Soret spectrum of MbO_2* as it cools and narrows. Since the Soret band area is fixed, the narrowing line shape leads to absorption from the MbO_2* species that increases at 420 nm (thus reducing the magnitude of the initial bleaching signal). The opposite effect (i.e., a decrease in absorption) observed in the wings of the absorption band (e.g., between 400 and 410 nm) confirms the narrowing (and cooling) of the MbO_2* Soret band in the first few picoseconds following excitation.

The MbNO sample (Figure 1D) presents a more complicated signal because both geminate ligand recombination and cooling are taking place simultaneously. Since it turns out that the quantum yield for ligand photolysis is twice as large for MbNO compared to MbO_2 (see below), the signals from the cooling

(28) Tian, W. D.; Sage, J. T.; Srajer, V.; Champion, P. M. *Phys. Rev. Lett.* **1992**, *68*, 408−411.

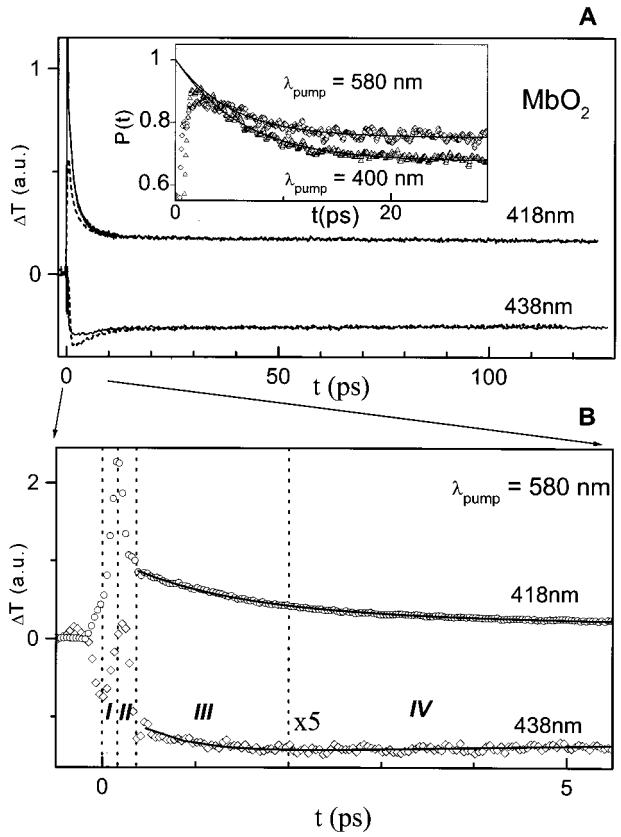

Figure 2. Optical response of MbO_2 probed at the Soret peaks of the reactant (418 nm) and product (438 nm). Panel A: solid line is for a 580-nm pump and the dashed line is for a 400-nm pump. Panel B: an enlargement of the 580-nm pump data showing the first 5 ps in more detail. The inset in panel A represents the survival probability, $P(t)$, and shows the response at 438 nm inverted and normalized to unity for 580- (diamond) and 400-nm pumps (triangle). The $P(t)$ axis is truncated at 0.6.

of the six-coordinate species are only half as large in MbNO as in MbO_2. Similarly, the initial bleaching and antibleaching signals (point i above) are twice as large for MbNO compared to MbO_2. Such effects are qualitatively evident, when the relative amplitudes of the signals in Figure 1C and D are compared.

Ultrafast Dynamics. The ligated heme protein samples appear to have a similar ultrafast response in the first 300−400 fs. To illustrate this response in more detail, we consider the high-resolution MbO_2 optical response shown in Figure 2. An enlargement of the signal in the first 5 ps, following a 580-nm pump of the MbO_2 sample, is shown in Figure 2B. The transient signals at 418 and 438 nm are fit between 400 fs and 20 ps, using two exponentials and a constant offset, and are shown as the solid lines, with parameters given in Table 1. The ultrafast optical response shows some clear turning points that can be used to divide the signal into four general regions: (I) 0−160 fs is within the system response of ∼200 fs and shows the initial bleach of the reactant material at 418 nm (combined with the coherent coupling signal); (II) 160−360 fs shows the simultaneous decay of reactant bleach and the rise of the product antibleach; (III) 360 fs−2 ps shows a decay of reactant bleach with ∼1-ps time constant along with a smaller rise in the antibleach; (IV) 2−20 ps shows a decay with a 4-ps time constant in both the reactant bleach and the product antibleach (see inset in Figure 2A).

Optical Response at the Soret Peaks. The optical response of metMb (Figure 3) is predominantly (94%) composed of a

Table 1. MbO_2: Parameters of Vibrational Relaxation and Geminate Recombination[a]

	λ_{probe} = 418 nm		λ_{probe} = 438 nm		assignment of optical response
λ_{pump}	τ_i (ps)	A_i	τ_i (ps)	A_i	
400 nm	1.1	1.22			MbO_2* VR
	4.3	0.51	6.0	−0.33	GR
	>200	0.49	>200	−0.67	BR
580 nm	1.0	1.94	1.1[b]	0.38[b]	MbO_2* VR
	4.8	0.59	4.1	−0.24	GR
	>200	0.41	>200	−0.76	BR

[a] The kinetics are fit using either one (at 438 nm) or two (at 418 nm) exponentials with an offset to account for the much slower bimolecular rebinding. The amplitudes and time constants are given using a normalization that is scaled so that the sum of the recombination amplitudes equals unity. The notation for the assignments is as follows: GR, geminate rebinding; BR, bimolecular recombination; VR, vibrational relaxation of indicated species. [b] When probing at 438 nm, the optical response in the 0.5−2-ps time window involves cooling signals from both the five-coordinate and six-coordinate species. However, due to the small quantum yield for MbO_2, contributions from MbO_2* are dominant.

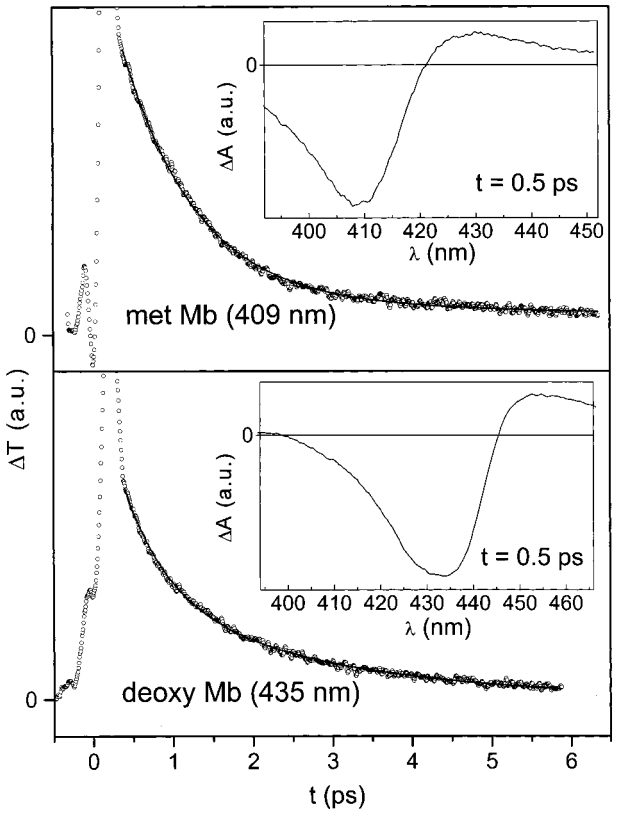

Figure 3. Optical response of metMb and deoxyMb probed at the Soret peaks (580-nm pump). Insets show the corresponding transient difference spectra at 0.5 ps. These spectra are consistent with broadening and red-shifting of the Soret transition due to vibrational heating of the electronic ground state. Exponential fits of the optical response at the Soret peaks yield τ_1 = 1.0 ps (94%), τ_2 = 20 ps (6%) for metMb and τ_1 = 0.5 ps (64%), τ_2 = 2.4 ps (36%) for deoxyMb.

1-ps relaxation process along with a small-amplitude (6%) slower phase (10−20 ps). The iron of metMb is known to bind a water molecule as the sixth ligand.[29] There appears to be no photodissociation of water molecules from the heme binding site, since no significant increase in absorbance is observed in the transient spectrum (not shown) between 390 and 395 nm at the position of the Soret peak of the five-coordinate ferric

(29) Quillin, M. L.; Arduini, R. M.; Olson, J. S.; Phillips, G. N., Jr. *J. Mol. Biol.* **1993**, *234*, 140−155.

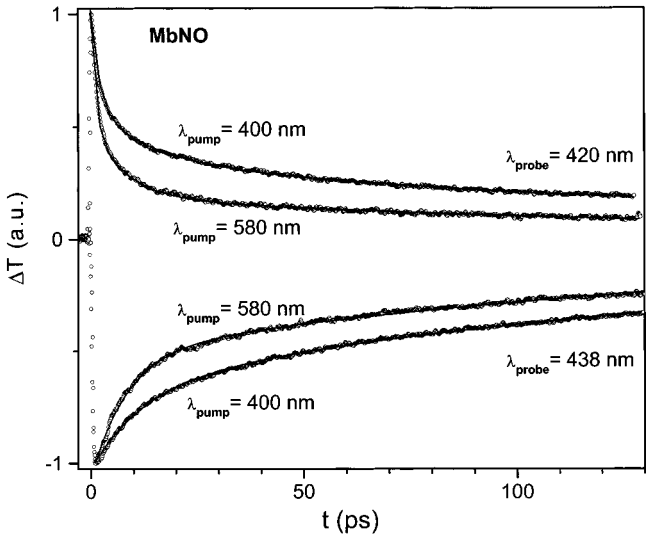

Figure 4. MbNO optical response probed at Soret peaks of reactant (420 nm) and product (438 nm), and pumped at 400 and 580 nm. Fits to the data are given in Table 2 and start at 400 fs to avoid coherent coupling effects.

myoglobin species.[30] The transient spectra of metMb and deoxyMb at 0.5 ps show a similar red-shifted hot band. We assign the 1-ps relaxation of metMb to the cooling of the six-coordinate heme group. The optical response of deoxyMb (Figure 3) differs from metMb in that the relaxation at the Soret peak cannot be fit with a single exponential. A two-exponential fit with time constants of 0.5 (64%) and 2.4 ps (36%) is shown in the lower panel of the figure.

As seen in Figure 1C and in Figure 2A, MbO_2 shows no evidence of geminate recombination from 20 to 120 ps, independent of pump wavelength. At the Soret peak of the reactant (418 nm), we find a large optical decay that takes place with a ~1-ps time constant and a smaller component of the decay that takes place with a 4−5-ps time constant (see Table 1). When probed at the Soret peak of the photoproduct (438 nm), the 4−6-ps decay is more prominent and of opposite sign relative to the ~1-ps process (see Table 1 and the inset in Figure 2A). The relative signs of the 4−6-ps processes observed at 418 and 438 nm are consistent with the assignment of this response to geminate recombination.

MbNO also shows an initial large-amplitude decay of the reactant bleach with a ~1-ps time constant (Figure 4, Table 2). This signal occurs when the system is probed at 420 nm, but not at 438 nm, indicating that the 1-ps response is associated with the residual six-coordinate species. The MbNO geminate recombination, which appears in both the bleach and antibleach signals (as it must), cannot be fit using a single exponential although adequate fits are found using two-exponential time constants, one between 8 and 13 ps and the other between 170 and 200 ps. These results agree qualitatively with previous work.[31,32] However, we do find a trend in the kinetics that indicates a dependence on the pump wavelength. Pumping at 400 nm yields both a smaller amplitude and rate for the fast geminate rebinding phase compared to pumping at 580 nm. This can be seen directly in the data of Figure 4 where the kinetics (and fits) at different pump wavelengths are compared.

Table 2. MbNO: Parameters of Vibrational Relaxation and Geminate Recombination[a]

	λ_{probe} = 420 nm		λ_{probe} = 438 nm		assignment of optical response
λ_{pump}	τ_i (ps)	A_i	τ_i (ps)	A_i	
400 nm	1.8	0.72			MbNO* VR
	13.8	0.41	13.0	−0.35	GR
	200	0.59	190	−0.65	GR
580 nm	1.1	1			MbNO* VR
	8.0	0.60	8.3	−0.50	GR
	170	0.40	170	−0.50	GR

[a] The kinetics are fit using either two (at 438 nm) or three (at 420 nm) exponentials with no offset. The amplitudes and time constants are given using a normalization that is scaled so that the sum of the geminate recombination amplitudes equals unity. The notation for the assignments is as follows: GR, geminate rebinding; VR, vibrational relaxation of indicated species.

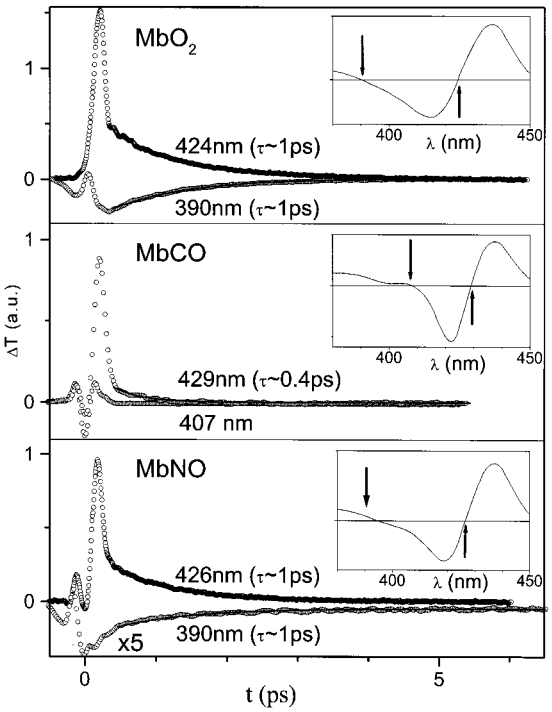

Figure 5. Optical response measured at the equilibrium isosbestic points for MbCO, MbO_2, and MbNO (pumped at 580 nm). Insets show the equilibrium difference spectra between deoxyMb and the corresponding ligated species, with the arrows showing the probe positions. Fits to the data start at 400 fs to avoid coherent coupling effects. The data at the isosbestic points of MbO_2 and MbNO are well fit with a single exponential with a ~1-ps time constant. The MbCO data show a weak response at 429 nm with a time constant of 0.4 ps.

Optical Response at the Equilibrium Isosbestic Points. Isosbestic points are the spectral positions where the reactant and product have the same absorption cross section. At these wavelengths, the geminate recombination contribution to the signal will be nearly zero. In Figure 5, the MbNO and MbO_2 samples show a similar 1-ps process at both the "red" and "blue" isosbestic points (relative to the reactant Soret band bleach) depicted by the arrows in the insets. MbCO shows a small bleaching signal relaxation (~0.4 ps) at the "red" isosbestic point between the reactant and product Soret peaks. The "blue" isosbestic points of MbO_2 and MbNO show an initial antibleach, while that of MbCO shows no signal in this region.

(30) Cao, W.; Christian, J. F.; Champion, P. M.; Rosca, F.; Sage, J. T. *Biochemistry* **2001**, *40*, 5728−5737.
(31) Petrich, J. W.; Lambry, J. C.; Kuczera, K.; Karplus, M.; Poyart, C.; Martin, J. L. *Biochemistry* **1991**, *30*, 3975−3987.
(32) Kholodenko, Y.; Gooding, E. A.; Dou, Y.; Ikeda-Saito, M.; Hochstrasser, R. M. *Biochemistry* **1999**, *38*, 5918−5924.

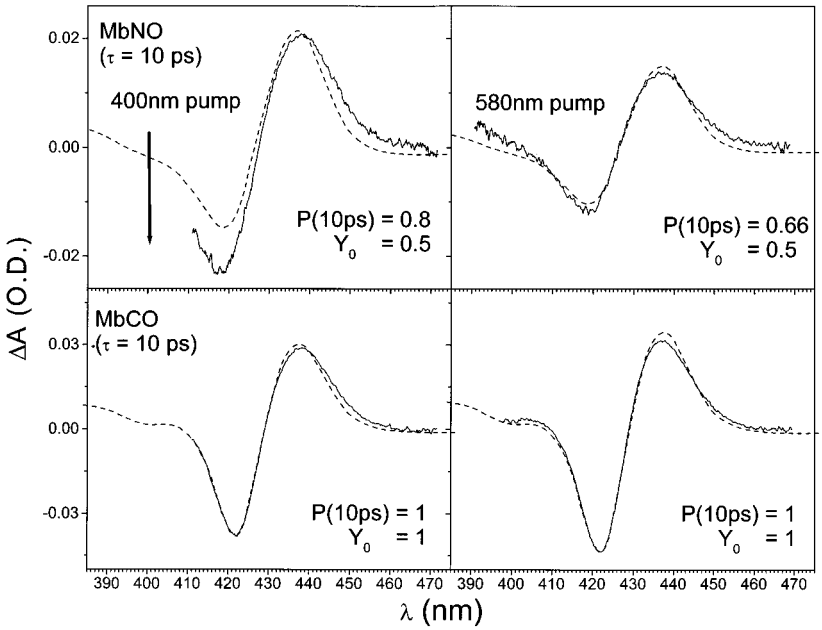

Figure 6. Quantum yield of MbNO. The solid lines are transient spectra of MbNO and MbCO at 10 ps, and the dashed lines are scaled equilibrium difference spectra of deoxyMb and MbNO (or MbCO). The ordinate is given in units of optical density (OD). The scaling factor for MbNO is calculated according to the text by using MbCO as a reference and takes into account the pump wavelength-dependent geminate recombination, P(10 ps), and the quantum yield, Y_0. The left and right side panels show results for 400- and 580-nm pumping, respectively. The distortion near 420 nm for the spectra pumped at 400 nm is due to leakage of pump light into the detector.

Quantum Yield. MbNO, as shown in Figure 6, is found to have an initial ($t \sim 0$) quantum yield $Y_0 = 0.5$, which is independent of the 400 and 580-nm pump wavelengths. The quantity P(10 ps) refers to the deoxyMb survival probability extrapolated from $t = 0$ to 10 ps and represents the fraction of the photodissociated population that has not undergone geminate recombination in the first 10 ps. The pump wavelength independence suggests that a common state (to the red of 580 nm) is involved in ligand dissociation and internal conversion to ground state. The quantum yield is deduced by use of MbCO as a reference. The MbCO transient signal is compared to the MbCO equilibrium difference spectrum as shown in the lower panels of Figure 6. The comparisons of the equilibrium difference spectra (dashed lines) with the transient difference spectra (solid lines) are made at 10 ps, so that heating and cooling effects are suppressed. Since the quantum yield of MbCO is unity,[26,27] the scaling factor needed to adjust the equilibrium difference spectrum to fit the data can obtained directly from the measurements in the lower panels (this accounts for experimental factors such as beam overlap, amount of sample photolysis, etc.). When the MbNO equilibrium difference spectrum is scaled by the same factor (after corrections for small differences in sample optical density) and compared to the MbNO transient signal at 10 ps, we find that the measured difference spectrum is smaller than predicted by the equilibrium difference. In order to take into account the reduction in photolyzed material at 10 ps due to geminate recombination, we scale the amplitude of the equilibrium difference spectrum downward by P(10 ps) as determined from the parameters in Table 2. However, an additional reduction factor is needed to fit the measured difference spectrum and this determines the intrinsic quantum yield for MbNO (i.e., in this case $Y_0 = 0.5$). Note that the data obtained using the 400-nm pump wavelength suffer from a small amount of leakage into the detector between 400 and 420 nm, which distorts the agreement between the transient and equilibrium line shapes in this region.

As noted above, the effect of geminate recombination is accounted for by extrapolating to $t = 0$. The reduction in population of the initially photolyzed material, P(10 ps), can be found using the time constants and amplitudes given in Table 2, (i.e., P(10 ps) = 0.8 for 400-nm pump and P(10 ps) = 0.66 for 580 nm pump). Thus, the final scaling of the MbNO equilibrium difference spectrum to match the transient difference spectrum takes into account the amount of sample excitation (using MbCO as a reference), the amount of geminate recombination extrapolated from $t = 0$ to the measurement time (using P(10 ps)), and a $t \sim 0$ quantum yield (Y_0) that is less than unity. For MbNO, this yield is found to be 50 ± 5%. The different values for P(10 ps) at the 400- and 580-nm pump wavelengths result from the pump wavelength-dependent geminate recombination amplitudes. This pump wavelength dependence of the kinetics can be discerned directly from the data in Figure 4.

A similar procedure is used for MbO_2 (Figure 7), which is found to have a 26% quantum yield using the 580-nm pump pulse and a 34% quantum yield using the 400-nm pump. Here, we have taken the entire (pump wavelength-dependent) decay, associated with the ~4−6-ps time constant that is measured at the Soret peak of the product state (see inset of Figure 2A), to be due to geminate recombination. It is important to note that this decay has the appropriate sign for geminate recombination and is opposite in sign to the 2.4-ps cooling signal measured at the Soret peak of deoxyMb (see Figure 3). We utilize the kinetic measurements at the Soret peak of the product state (438 nm) to reconstruct the fast component of geminate recombination in MbO_2 in order to minimize interference from the cooling of the unphotolyzed six-coordinate MbO_2* state. Even after doing this, we believe that the small wavelength dependence found

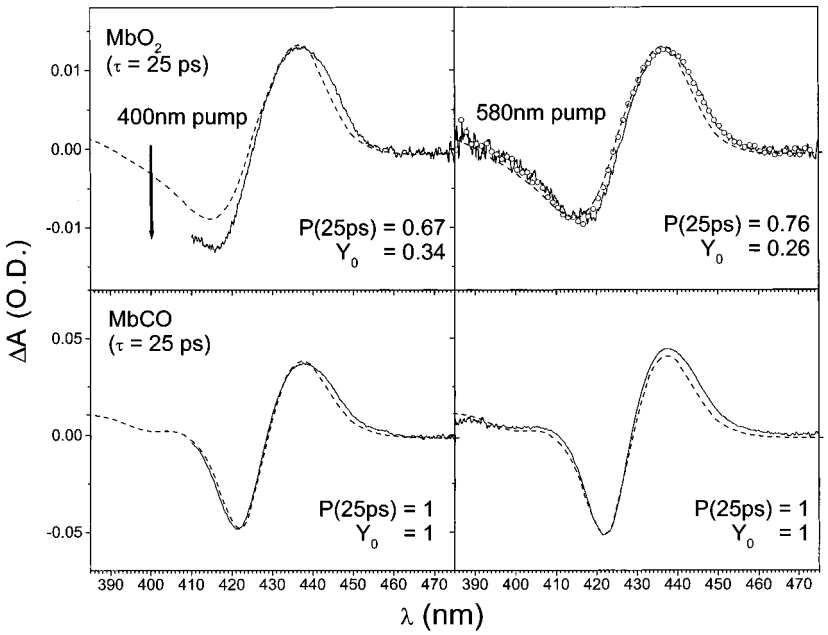

Figure 7. Quantum yield of MbO_2. The left and right side panels show results for 400- and 580-nm pumping, respectively. The distortion near 420 nm for the spectra pumped at 400 nm is due to leakage of pump light into the detector. In the 580-nm pump experiment, the solid lines correspond to samples at pH 7 and the circles are for samples at pH 5. The transient spectra of MbO_2 and MbCO are measured at 25 ps, and the dashed lines are the scaled equilibrium difference spectra of deoxyMb and MbO_2 (or MbCO). The ordinate is given in units of optical density (OD). The scaling factor for MbO_2 is calculated according to the text by using MbCO as a reference and takes into account the geminate recombination, P(25 ps), and the quantum yield, Y_0.

in the quantum yield for MbO_2 arises from uncertainties in the extrapolation of the geminate rebinding to $t = 0$ (see inset in Figure 2A).

Another difficulty is that the optical response measured at 438 nm may also contain components that arise from cooling of the Mb* state. However, since the ~4-ps decay of the antibleaching signal at 438 nm coincides with a ~4-ps decay of the bleaching signal at 418 nm, this is a strong indication that a significant component of this signal arises from geminate recombination. To set limits on the quantum yield, we take the amplitude of the ~4−6-ps process to be either partially (50%) or completely (100%) due to geminate recombination. This gives a range of 22−26% for the quantum yield using the 580-nm pump pulse and a range of 27−34% for the quantum yield using the 400-nm pump. As a conservative result, we take 28 ± 6% as the most probable overall range for the MbO_2 quantum yield.

As a final observation, we note that the quantum yields of MbO_2 at pH 5 (open circles in Figure 7) and at pH 7 (solid line) are essentially the same.

Discussion

Subpicosecond Optical Response. The bleaching of the reactant (process I) takes place within system response time and is consistent with photodissociation on time scales in the range of ~60−70 fs, which correspond to the oscillatory periods ($T = 1/c\tilde{\nu}$) of the Fe−L stretching and bending modes: $\nu_{Fe-CO} \sim 512$ cm^{-1}; $\Delta_{Fe-C-O} \sim 577$ cm^{-1}; $\nu_{Fe-NO} \sim 554$ cm^{-1}; $\delta_{Fe-N-O} \sim 449$ cm^{-1}; $\nu_{Fe-O2} \sim 568$ cm^{-1}; $\delta_{Fe-O-O} \sim 425$ cm^{-1}.[33] The rise of the antibleaching signal (process II) is delayed by ~300 fs from that of the bleaching signal. This 300-fs optical response is consistent with intramolecular vibrational energy redistribution of the photolyzed heme, although a detailed analysis is complicated by the coherence coupling signal from the solvent. As the hot product state (five-coordinate heme) cools, the extremely broad early time deoxy Soret absorption band narrows and the absorption at 438 nm increases, leading to the appearance of the 300-fs response. An analysis of the full spectral evolution using white light continuum probe pulses and absorption line shape simulations is quantitatively consistent with a cooling model for the 300-fs response.[21]

Vibrational Relaxation of Six-Coordinate Heme. The optical response of metMb after photoexcitation shows a ~1-ps signal associated with the vibrational relaxation of the six-coordinate heme. The optical response of MbNO and MbO_2 at the Soret peak of the ligand-bound state also consists of a dominant ~1-ps relaxation, which suggests that the cooling process for the six-coordinate heme group may be relatively insensitive to the nature of the sixth ligand. The ~1-ps time constant contrasts with the measurements on the unligated (deoxy) heme, which are fit using a biphasic response with time constants of ~0.5 and ~2.4 ps when probed at the Soret peak (e.g., see Figure 3).

As can be seen from Figure 5, the optical response at the isosbestic points is very different for MbCO than for MbNO and MbO_2. The response shows a major ~1-ps component for MbO_2 and MbNO at the red and blue isosbestic points, while this signal is almost absent in MbCO. Since the reactant and dissociated product in equilibrium have the same absorption at the isosbestic points, the 1-ps relaxation process at the isosbestic wavelengths could potentially arise from a transient species. Previous studies[9] have led to an excited-state model with red-shifted intermediate electronic states characteristic of unligated heme absorbing near ~460 nm. In this model, it is suggested that ligand rebinding of NO and O_2 within 2 ps is a major

(33) Kincaid, J. Resonance Raman Spectra of Heme Proteins and Model Compounds. In *The Porphyrin Handbook*; Kadish, K. M., Smith, K. M., Guilard, R., Eds.; Academic Press: San Diego, CA, 2000; Vol. 7, pp 225−292.

component of the kinetics. However, this model cannot explain the initial antibleach signal in MbO_2 and MbNO at the isosbestic point near 390 nm, unless still another (now blue-shifted) electronic intermediate state is postulated.

A much simpler explanation for the observed optical response is that the electronic ground state of the *ligated* heme is vibrationally excited (i.e., hot). A hot six-coordinate ground state shows a broadened Soret band spectrum, which accounts for the initial antibleach and ~1-ps decay in the wings of the Soret peak near the 390-nm isosbestic point. Since MbCO has a unity quantum yield, its photoproduct states are all dissociated so no hot ligand-bound state is created, and the signals at the blue isosbestic point (407 nm) are absent. On the other hand, the dissociated heme is vibrationally excited, and its relaxation (narrowing and blue shifting) contributes to the small bleaching decay (~0.4 ps) at the equilibium isosbestic point near 429 nm in MbCO (Figure 5).

Geminate Recombination of MbNO. The geminate recombination of NO cannot be explained with a single-exponential process. The MbNO system shows two dominate geminate rates, one near 10 ps and the other near 200 ps (see Table 2). This agrees with prior observations.[32] However, we also note that the amplitude and rate of the fast rebinding phase appear to distinctly depend on the pump photon energy (Figure 4). Pumping at 400 nm generates a smaller amplitude and rate for the fast geminate recombination than pumping at 580 nm. One conceivable explanation is that the vibrational excitation of Mb^* affects the geminate ligand recombination rate. Since the dissociated heme is hot initially, it may have an affinity for the ligand that is smaller initially but increases as the deoxyheme cools. With more pump energy at 400 nm, the initial heme temperature will be higher, which would lead to a less efficient geminate rebinding process. For example, it has been suggested that heating of the heme group increases the iron out-of-plane distance, due to anharmonicities in the potential surface.[34] Since it was previously suggested[35] that the iron displacement contributes significantly to the geminate rebinding barrier height, the role of transient heme heating may prove to be important in understanding the initial stages of NO geminate recombination.

Geminate Recombination of MbO_2. The lack of a ~4-ps process at the isosbestic points of MbO_2, and its presence at both 418 and 438 nm, suggests that this signal arises primarily from a geminate recombination process. However, the relative amplitude of the ~4-ps decay is different at the two probe wavelengths, which suggests that some degree of spectral dynamics (e.g., due to heme cooling) may be mixed in with the ~4-ps geminate recombination. The uncertainty in the relative proportion of geminate recombination and spectral dynamics that comprise the ~4-ps response is reflected in the extrapolation of the survival probability between $t = 0$ and the measurement time (25 ps for MbO_2). If the entire amplitude of the ~4-ps signal is taken to be due to population changes arising from geminate recombination, this leads to a quantum yield for MbO_2 that depends more strongly on pump wavelength. Since it seems likely that some of the 4-ps optical response is due to cooling of the hot heme, we have given a range for Y_0 that reflects an assumption that 50−100% of the ~4-ps process is due to geminate recombination.

Electronic Structure, Bonding Geometry, and Quantum Yield. The bonding of a diatomic molecule XY with a transition metal complex has been studied extensively. The bending of the MXY unit is intrinsically correlated with the orbital overlaps between the diatomic molecule and the metal atom, and the bend angle is suggested to be determined by the relative strength of the ($d_{z^2} - \pi^*$) σ-bonding, d_{z^2}−lone pair interaction, and π back-bonding.[36−38] A general relation is observed[36] for the geometry of a metalloporphyrin (M) and diatomic ligand (XY) complex $\{M-XY\}^r$, which depends on r, the sum of electrons associated with the metal d and ligand π^* or σ^* orbitals. The M−X−Y linkage is linear when $r \leq 6$ and has a bent end-on configuration when r is greater than 6. For example, for ferrous myoglobin, $r = 6$, 7, and 8 for MbCO, MbNO, and MbO_2, respectively. Consistent with this prediction, recent infrared and xray crystallographic measurements have shown that Fe−CO is almost linear,[39,40] while Fe−O_2 and Fe−NO have bent configurations.[41,42]

Photosensitivity studies of liganded hemoproteins noticed a similar correlation with photolability. That is, linear, formally d^6, metal−ligand fragments are relatively photolabile, and bent, higher electron occupancy fragments are relatively photoinert.[43] However, these studies were unable to take into account the effect of ligand geminate recombination and the asserted "quantum yield" (which is actually bimolecular dissociation yield) was suggested to be of order $\sim 10^{-3}$ for MbNO and $\sim 10^{-2}$ for MbO_2. The present studies conclude that the ($t \sim 0$) intrinsic photodissociation quantum yields of MbCO, MbNO, and MbO_2 are ~1.0, 0.5, and 0.3, respectively.

Vibrational interaction theory[34,44] presents a systematic approach to establish the correlation between the electronic structure, bonding geometry, and photoreactivity. For a heme−diatomic ligand complex with a highly symmetric linear bonding geometry, there is a possible instability due to the pseudo Jahn−Teller effect, which distorts the linear configuration along a bending normal mode. If vibronic mixing of the ground and low-lying excited states of the linear configuration is above a critical value, the pseudo Jahn−Teller effect will cause the symmetry of the original ground state to be broken and the ground-state minimum will shift along the vibronically active bending normal coordinate. A vibronic mixing analysis of the molecular orbitals $e(d_\pi \pm \pi^*_L)$ (which are metal−ligand bonding and antibonding π-orbitals) and $a_1(d_{z^2})$ (which contributes predominantly to the metal−axial ligand σ-bonding) with respect to the normal coordinate associated with ligand bending successfully accounts for the ground-state bonding geometry of MbCO, MbNO, and MbO_2.[34]

(34) Bersuker, I. B.; Stavrov, S. S. *Coord. Chem. Rev.* **1988**, *88*, 1−68.
(35) Srajer, V.; Reinisch, L.; Champion, P. M. *J. Am. Chem. Soc.* **1988**, *110*, 6656−6670.
(36) Yu, N. T.; Kerr, E. A. *Biological Applications of Raman Spectroscopy*; Wiley-Interscience Publication: New York, 1988; Vol. 3, pp 39−95.
(37) Li, X. Y.; Spiro, T. G. *J. Am. Chem. Soc.* **1988**, *110*, 6024−6033.
(38) Vogel, K. M.; Kozlowski, P. M.; Zgierski, M. Z.; Spiro, T. G. *J. Am. Chem. Soc.* **1999**, *121*, 9915−9921.
(39) Ivanov, D.; Sage, J. T.; Keim, M.; Powell, J. R.; Asher, S. A.; Champion, P. M. *J. Am. Chem. Soc.* **1994**, *116*, 4139−4140.
(40) Yang, F.; Phillips, G. N., Jr. *J. Mol. Biol.* **1996**, *256*, 762−774.
(41) Phillips, S. E. V.; Schoenborn, B. P. *Nature* **1981**, *292*, 81−82.
(42) Rich, A. M.; Armstrong, R. S.; Ellis, P. J.; Lay, P. A. *J. Am. Chem. Soc.* **1998**, *120*, 10827−10836.
(43) Hoffman, B. M.; Gibson, Q. H. *Proc. Natl. Acad. Sci. U.S.A.* **1978**, *75*, 21−25.
(44) Enemark, J. H.; Feltham, R. D. *Coord. Chem. Rev.* **1974**, *13*, 339−406.

Since the $\pi \rightarrow \pi^*$ Soret excitation places an electron into one of the e_u porphyrin orbitals, the mixing of this electron density with the Fe−L antibonding (d_{z^2}) orbital is presumably a key step in the photolysis reaction. Vibronic mixing of the porphyrin e_u and iron d_{z^2} orbitals requires a mode of e symmetry, and it has been suggested that the Fe−L bending modes are the dominant symmetry-allowed modes leading to ligand bending distortions and dissociation in the excited state.[34] Within this picture, the linear CO binding geometry leads to an excited-state species that is far from equilibrium along the bending coordinate. In contrast, the NO and O_2 ligands are already in a bent configuration in the ground state, so they are much closer to equilibrium in the excited state and photodissociation is less likely. Conceivably, the differences in relative ground-state binding geometry (O_2 is more bent than NO) could also help to account for the ligand-dependent quantum yields measured in this study.

However, one might expect that the resonance Raman intensities of the bending modes would also reflect the ligand-specific differences between the ground- and excited-state equilibrium positions along the bending coordinate. Unfortunately, restrictive selection rules and competition from strong Franck−Condon allowed scattering in the Soret band leads to Raman bending transitions that are weak and difficult to observe.[33] On the other hand, the resonance Raman spectra do reveal that, for the ν_{Fe-L} stretching modes (L = CO, NO, O_2), Fe−CO has a significantly higher intensity than Fe−O_2 and Fe−NO. This difference is probably due to a combination of the electronic structure and the Fe−L binding geometry. One possibility is that the weaker resonance Raman coupling for Fe−L modes in the bent ligand binding geometry is an indirect reflection of smaller displacements along the bending coordinate following electronic excitation (such an effect could arise from Duschinsky mixing of the bending and stretching modes in the excited state). Taken together, the data appear to be consistent with the hypothesis[34] that distortions along the bending coordinate play a crucial role in the photodisssociation process. An interesting, and potentially related, observation by Anfinrud et al.[45] is the appearance of the CO dipole within ∼0.5 ps of photolysis, orientated parallel to the heme plane. Such a rapid (90°) change in the ligand orientation would obviously be facilitated, if dissociation takes place along the ligand bending coordinate.

Unphotolyzable Conformation. In low-temperature photodissociation studies, Chance et al.[46] found two conformations of MbO_2. Roughly 50% of the MbO_2 population at pH 7 was found to be photolyzable at 10 K, while the rest of the population was not photolyzable, even using multiple photon photoexcitation with a cw laser. Moreover, it was found that the photolyzable population was reduced to 18% at pH 5.[47] Given these results, we wondered whether these same two conformations persist at room temperature and affect the initial quantum yield measurements. The answer seems to be no. Our results show that, at room temperature, the quantum yield for O_2 photolysis is the same at pH 5 and pH 7 (Figure 7). Moreover, the observation that an intense nanosecond pulse generates more dissociation products than a picosecond pulse[11] suggests that the conformations having the different quantum yields interconvert rapidly ($\leq$ ns) at room temperature (i.e., multiple photoexcitations within the nanosecond pulse can access both conformations). Also, MbNO can be completely photodissociated at low temperature using multiple photoexcitations,[48] which means that there is no unphotolyzable population in this case. Thus, it is unlikely that an unphotolyzable fraction is the source of the 50% quantum yield measured for MbNO at room temperature.

On the other hand, the possibility of a photomediated transition between two conformations may be connected to the much lower quantum yield of MbO_2. For example, infrared studies[49] on the dioxygen adducts of iron(II) porphyrin suggest two isomeric dioxygen adducts exist at 15 K. As temperature increases, one isomer becomes unstable and changes to the other isomer.[49] The isomer that is unstable at higher temperature (100 K) is assigned to have a side-on binding geometry between oxygen and iron, while the other conformation is assigned to have a bent end-on configuration.[49] A theoretical study of oxymyoglobin also indicates two energy minimums corresponding to the bent end-on and perpendicular side-on structures,[50] with hydrogen bonding between oxygen and vicinal ligands favoring the bent end-on conformation.

These results suggest the possibility that the side-on structure (which has no bending coordinate) may represent the unphotolyzable fraction observed by Chance et al. at low temperature.[46] One scenario that might account for the reduction in quantum yield of MbO_2 compared to MbNO at room temperature involves photomediated branching transitions to the side-on structure, which must lie quite close in energy to the more stable end-on ground state. Such branching transitions to the side-on structure would obviously be facilitated if, upon the $\pi \rightarrow \pi^*$ electronic excitation, the system distorts along the bending coordinate. As electron density is mixed into the Fe−L antibonding orbital, the system can either dissociate or branch to the side-on structure (followed by rapid relaxation to the "hot" end-on electronic ground state).

Conclusions and Summary

We arrive at the following picture of the ligand photodissociation process for O_2 and NO. Following photoexcitation of either MbO_2 or MbNO, there are rapid (<300 fs) internal conversion processes that return a significant fraction of the system to the initial six-coordinate ground electronic state (∼50% for MbNO and ∼72% for MbO_2). This results in a "hot" ligand-bound heme system that contributes to the transient optical response with a ∼1-ps time constant, as the six-coordinate heme system cools. The six-coordinate metMb sample shows very similar (∼1 ps) behavior with no detectable photodissociation. This should be contrasted with the optical response of the five-coordinate deoxyheme, which displays a distinctly biphasic signal with time constants of ∼0.5 and ∼2.4 ps when monitored at the peak of the Soret band (see Figure 3).

(45) Lim, M.; Jackson, T. A.; Anfinrud, P. A. *Science* **1995**, *269*, 962−966.
(46) Chance, M. R.; Courtney, S. H.; Chavez, M. D.; Ondrias, M. R.; Friedman, J. M. *Biochemistry* **1990**, *29*, 5537−5545.
(47) Miller, L. M.; Patel, M.; Chance, M. R. *J. Am. Chem. Soc.* **1996**, *118*, 4511−4517.
(48) Miller, L. M.; Pedraza, A. J.; Chance, M. R. *Biochemistry* **1997**, *36*, 12199−12207.
(49) Watanabe, T.; Ama, T.; Nakamoto, K. *J. Phys. Chem.* **1984**, *88*, 440−445.
(50) Bertran, J.; Ruizlopez, M. F.; Rinaldi, D. *Theochem* **1991**, *232*, 337−347.

An important theoretical question raised by the current study concerns the origin of the distinctly different cooling behavior found for the five- and six-coordinate heme systems. One possibility is that the "domed" geometry of the five-coordinate deoxyheme and the planar six-coordinate ligand-bound structure couple very differently to the protein environment. Such differences in coupling have revealed themselves in the substantially different magnitude of inhomogeneous broadening needed to quantitatively account for the Soret band line shapes of the five- and six-coordinate heme systems.[51]

In the case of O_2 and NO photodissociation, only ~28% of the MbO_2 or ~50% of the MbNO complete the bond breakage event, leaving a hot five-coordinate heme with a dynamic Soret band spectral signature that narrows (300−400 fs) and shifts (~2−4 ps) as the system cools.[21] The MbNO system displays both a rapid (~10 ps) and a slow (~200 ps) phase of nearly complete (>95%) geminate rebinding, while MbO_2 undergoes a small amplitude (20−30%) geminate process with a time constant of ~4 ps that may also contain components of a deoxyheme cooling signal. The relative amplitudes and rates for geminate rebinding in MbNO are pump wavlength dependent (Figure 4), suggesting that the initial heme temperature following photoexcitation may influence the geminate rebinding process. Finally, we note that the results for MbNO and MbO_2 stand in marked contrast to MbCO, which dissociates with unity quantum yield so that no six-coordinate heme cooling can be observed.

These results are consistent with the hypothesis that an excited-state ligand bending distortion plays a role in the dissociation process. This distortion is much larger for the CO ligand, due to its linear ground-state binding geometry, resulting in a quantum yield near unity. Since both the NO and O_2 ligands bind in a bent conformation, the significant reduction in the MbO_2 quantum yield compared to MbNO is potentially related to the existence of a transient side-on binding geometry for O_2. At low temperature we suggest that this structure is stabilized and unphotolyzable, while at room temperature this structure could be transiently accessed as the system distorts along the ligand bending coordinate. This offers the possibility for rapid branching into the ground electronic-state manifold and leads to a reduction in the probability of O_2 dissociation.

Acknowledgment. This work was supported by grants from NIH (DK35090) and NSF (MCB9904516).

JA017359N

(51) Srajer, V.; Schomacker, K. T.; Champion, P. M. *Phys. Rev. Lett.* **1986**, *57*, 1267−1270.